Molecular Therapy
Methods & Clinical Development
Original Article

# Toxicology Study of Intra-Cisterna Magna Adeno-Associated Virus 9 Expressing Iduronate-2-Sulfatase in Rhesus Macaques

Juliette Hordeaux,[1] Christian Hinderer,[1] Tamara Goode,[1] Elizabeth L. Buza,[1] Peter Bell,[1] Roberto Calcedo,[1] Laura K. Richman,[1] and James M. Wilson[1]

[1]Gene Therapy Program, Department of Medicine, University of Pennsylvania, Perelman School of Medicine, Philadelphia, PA 19104, USA

**Hunter syndrome is an X-linked recessive disease caused by deficiency of the lysosomal enzyme iduronate-2-sulfatase. The severe form of this progressive, systemic, and neurodegenerative disease results in loss of cognitive skills and early death. Several clinical trials are evaluating adeno-associated virus 9 for the treatment of neurodegenerative diseases using systemic or intrathecal lumbar administration. In large animals, administration via suboccipital puncture gives better brain transduction than lumbar administration. Here, we conducted a good laboratory practice-compliant investigational new drug-enabling study to determine the safety of suboccipital adeno-associated virus 9 gene transfer of human iduronate-2-sulfatase into nonhuman primates. Thirteen rhesus macaques received vehicle or one of two doses of vector with or without immunosuppression. We assessed in-life safety and immune responses. Animals were euthanized 90 days post-administration and sampled for histopathology and biodistribution. The procedure was well tolerated in all animals. Minimal mononuclear cerebrospinal fluid pleocytosis occurred in some animals. Asymptomatic minimal-to-moderate toxicity to some dorsal root ganglia sensory neurons and their associated axons occurred in all vector-treated animals. This study supports the clinical development of suboccipital adeno-associated virus 9 delivery for severe Hunter syndrome and highlights a potential toxicity that warrants monitoring in first-in-human studies.**

## INTRODUCTION

Mucopolysaccharidosis type II, also known as Hunter syndrome, is an X-linked lysosomal storage disease with an estimated incidence of 1.3 in 100,000 male newborns.[1] The disease is caused by a deficiency in the enzyme iduronate 2-sulfatase (IDS), which leads to an accumulation of undegraded glycosaminoglycans (GAGs) heparin and dermatan sulfate within lysosomes. This occurs in most cell types and tissues, including the airways, heart, liver, spleen, bones, joints, oropharynx, head, neck, leptomeninges, and CNS.[2] The severe form of Hunter syndrome is characterized by cognitive decline; patients with mild forms do not present with intellectual disability but can have specific deficits in attention and executive function.[3] The current approved treatment for Hunter syndrome is weekly intravenous enzyme replacement therapy (ERT, Elaprase Shire Human Genetic Therapies). This therapy ameliorates splenomegaly, hepatomegaly, and urinary GAGs in younger patients; it improves heart and auditory function but does not modify respiratory, eye, skeletal, or CNS symptoms.[1,4] Monthly intrathecal ERT is in the late phases of clinical trials. Phase I and II trials demonstrated a reduction of cerebrospinal fluid (CSF) GAGs; however, the administration device was associated with adverse events, some of which were severe.[5] As the CSF GAGs values obtained from mild (without cognitive impairment) versus severe Hunter syndrome patients can overlap, the impact of reducing CSF GAGs on cognitive function is unclear.[6]

CNS-directed intrathecal gene therapy is an alternative approach to provide high and sustained levels of enzyme to the brain with a single minimally invasive injection.[7–10] We recently conducted a pharmacology study of an adeno-associated virus (AAV) 9 vector expressing human IDS (hIDS) injected into a mouse model of Hunter syndrome. Following intracerebroventricular injection of vector, animals demonstrated dose-dependent IDS expression and clearance of the storage pathology in the brain, as well as improved long-term memory and novel object recognition.[9] These studies provided compelling data regarding the potential efficacy of AAV9 gene therapy with this product for Hunter syndrome.

Translation of these encouraging mouse-model pharmacology studies into humans requires critical assessment of the preferred route of administration. Administration of AAV vectors into the CSF can be performed via the lateral cerebral ventricles, similar to our mouse studies, or via a suboccipital or lumbar route. Suboccipital injection into the cisterna magna has been demonstrated to be more efficient than lumbar injection and safer than intracerebroventricular administration in large animals.[7] However, this approach is rarely utilized in the clinical practice, necessitating evaluation of the safety of the

Received 6 April 2018; accepted 7 June 2018;
https://doi.org/10.1016/j.omtm.2018.06.004.

**Correspondence:** James M. Wilson, MD, PhD, Gene Therapy Program, Perelman School of Medicine, University of Pennsylvania, 125 South 31st Street, Suite 1200, Philadelphia, PA 19104, USA.
**E-mail:** wilsonjm@upenn.edu

**Table 1. Study Design**

| Study | RGX161108p | | | RGX170213p | |
|---|---|---|---|---|---|
| Necropsy Day | 90 | | | 90 | |
| Group | 1 | 2 | 3 | 1 | 2 |
| Dose (GC) | vehicle | $5 \times 10^{13}$ | $1.7 \times 10^{13}$ | $5 \times 10^{13}$ | $1.7 \times 10^{13}$ |
| Immunosuppression | no | no | no | yes | yes |
| No. of animals | 1 | 3 | 3 | 2 | 3 |

procedure in preclinical studies. In order to advance this approach to the clinic, we performed a good laboratory practice-compliant toxicology study using adult rhesus macaques. We selected nonhuman primates for this study, as they are the preferred species for assessing vector-related immune toxicity.[11–13] Furthermore, the size and anatomy of nonhuman primates enables us to utilize the same image-guided intra-cisterna magna (ICM) delivery approach that would be employed in clinical studies.

## RESULTS

### Study Design

In this study, we utilized two experimental designs to evaluate the safety, biodistribution, and pharmacology of a vector encoding hIDS for up to 90 days after administration by ICM suboccipital puncture in rhesus macaques (Tables 1 and 2). In the first experiment, we evaluated a high dose (HD) of $5 \times 10^{13}$ genome copies (GCs; n = 3) and a low dose (LD) of $1.7 \times 10^{13}$ GCs (n = 3) compared to vehicle control (n = 1). The second experiment evaluated the two vector doses with a concurrent immune suppression (IS) regimen (n = 5). The regimen spanned from three weeks preinjection to day 60 for mycophenolate mofetil (MMF) and from preinjection to scheduled necropsy on day 90 for rapamycin.

### In-Life Safety Parameters

All animals survived until their scheduled necropsy at day 90 ± 3 days. The non-IS animals presented no clinical findings based on general observations, temperature, heart rate, and rate of breathing (recorded in sedated animals). Six animals received an IS regimen, which caused adverse effects of decreased appetite, diarrhea, and weight loss that all started prior to test article administration. These adverse effects led to the withdrawal of one animal from the HD group prior to test article dosing. Most of the affected animals tested positive for *Campylobacter* spp. and *Helicobacter* spp. based on culture or PCR testing of stools. We provided symptomatic care (sucralfate), supportive care (subcutaneous saline injections), and antibiotic treatments (erythromycin) to control the gastrointestinal symptoms. The remaining five animals received the test article treatment and were able to complete the study.

All animals maintained normal body weight throughout the study after receiving the test article (Tables S1 and S2). Before vector administration and during the IS stabilization phase, three animals had mild weight loss (200–350 g; 4%–6% of initial body weight). We attribute this to the gastrointestinal symptoms caused by IS drugs, the daily orogastric tubing required to administer the IS drugs, opportunistic enteric pathogens, or a combination of these factors.

### Pathology

Pathology consisted of periodic bleeds and CSF taps to gather complete blood cell (CBC) counts, blood chemistry and electrolyte panels, a coagulation panel (thromboplastin time, activated partial thromboplastin time, fibrinogen, D-dimers, fibrin degradation products), CSF white blood cell (WBC) counts, glucose and protein levels, and cytosmear analysis. We only present the parameters with test article-related modifications, defined as modifications that (1) exceeded the baseline average plus or minus two standard deviations, (2) occurred after administering the test article and (3) were not observed in the control group or historical control animals. We did not observe conclusive test-article-related abnormalities in CBC counts, blood chemistry (including transaminases), or coagulation parameters (data not shown) from non-IS animals. The five IS animals experienced modifications of their blood values after the onset of the IS regimen (Figure S1). These modifications first occurred prior to vector dosing and were thus unrelated to the test article. The IS animals presented with transient neutrophilic leukocytosis on day 0 and anemia that resolved after MMF withdrawal on day 60. Other parameters were normal with the exception of transient increases in some inflammatory markers, such as platelets, fibrinogen, and D-dimers. Furthermore, one LD IS animal showed increased transaminases (Figure S1). Gastrointestinal inflammation likely led to increases in some inflammatory markers. Albumin and phosphorus also trended low (Figure S1), likely due to intestinal malabsorption.

CSF analysis revealed treatment-related changes. A minimal mononuclear pleocytosis (5–20 cells per μL) occurred in 2/3 HD animals, 1/3 LD animals, and 1/3 LD IS animals (Figure 1 and Table S3). The vehicle controls showed normal CSF parameters throughout the study, although we excluded time points that showed blood contamination, which we defined as erythrocyte counts >500 cells/μL. The pleocytosis (mainly lymphocytes with fewer macrophages) appeared as early as day 21, peaked between days 21 and 45, and typically resolved by day 90, with only the LD IS animal having a late peak of pleocytosis on day 90, perhaps due to MMF withdrawal. In some animals, elevated CSF nucleated cells were inconsistently paralleled by a mild transient increase in CSF protein. We did not observe any changes in CSF glucose concentration.

### Immune Responses to hIDS and the AAV9 Capsid

We used an ELISA to evaluate serum and CSF samples for antibodies against hIDS (Figure 2A). We detected low levels of antibodies against hIDS in the serum of five animals: 3/3 HD animals, 2/3 LD animals, and 0/5 IS animals. We detected low levels of antibodies against hIDS in the CSF of three animals: 2/3 HD animals, 1/3 LD animals, and 0/5 IS animals. In these animals, the response peaked between days 30

**Table 2. Animals and Study Dates**

| Group | Animal No. | Gender | Weight (kg) | Vector Dose (GC) | IS Regimen | Blood + CSF Analysis | Urine + Stool Shedding | Necropsy |
|---|---|---|---|---|---|---|---|---|
| Vehicle | RA2198 | M | 3.90 | – | – | D0, D7, D14, D21, D30, D45, D60, D90 | D0, D5, D30, D90 | D90 |
| LD | RA1356 | M | 7.00 | $1.7 \times 10^{13}$ | – | | | |
| | RA1358 | M | 8.55 | | – | | | |
| | RA2197 | M | 4.75 | | – | | | |
| HD | RA1399 | M | 5.35 | $5 \times 10^{13}$ | – | | | |
| | RA2203 | M | 4.25 | | – | | | |
| | RA2231 | M | 4.35 | | – | | | |
| LD + IS | RA1442 | M | 5.55 | $1.7 \times 10^{13}$ | MMF + rapamycin 14 to 21 days preinjection–D60 rapamycin D60–D90 | | | |
| | RA2219 | M | 5.60 | | | | | |
| | RA2233 | M | 4.60 | | | | | |
| HD + IS | RA2201 | M | 4.80 | $5 \times 10^{13}$ | | | | |
| | RA2222 | M | 5.05 | | | | | |

Days 7–21 time points are ±1 day; days 5 and 30–60 are ±2 days; day 90 time point is ±3 days.

and 45 and subsequently decreased to levels that approached the limits of detection by day 90. Two LD animals and one HD animal did not develop detectable levels of antibodies in the CSF. One LD animal and all of the IS animals failed to develop detectable levels of antibodies in both the serum and CSF at the tested dilutions (1:1,000 and 1:20, respectively).

All animals showed a dose-dependent increase in AAV9 serum neutralizing antibodies (NAbs) starting on day 7, consistent with AAV vector administration (Figure 2B). The HD IS animals had lower serum NAb titers at all times compared to dose-matched non-IS animals. IS did not affect the LD group, which generally showed a weaker NAb response. NAb responses appeared later in the CSF, with lower titers than in sera, and were absent in all IS animals. Despite being prescreened negative to AAV9 NAbs, one LD IS animal (RA2233) seroconverted prior to vector dosing and had a baseline NAb titer of 1:40.

After vector dosing, only one LD animal had peripheral blood mononuclear cell (PBMC) T cell responses to the hIDS transgene (Figure 2C; Table S4). T cell responses to the AAV9 capsid occurred only in the LD IS group and persisted in only one animal.

### Histopathology

Peripheral organs exhibited no gross or histological test-article-related findings. We observed test-article-related histologic findings within the dorsal root ganglia (DRG) and the corresponding axons from the dorsal spinal cord white matter, sciatic nerve, and trigeminal nerve ganglia. Tables S5 and S6 list and summarize the incidence and severity of these findings.

Minimal to mild dose-dependent neuronal cell-body degeneration with mononuclear cell infiltration was present in at least one DRG and trigeminal ganglia of all animals (Figures 3A–3C), with the exception of one LD animal and the vehicle-treated control. Overall, the HD animals and the LD IS animals had the highest lesion severity. Grade 2 (mild lesion, 10%–25% of the tissue in an average high-power field) was the worst reported.

In spinal cord segments, a minimal (grade 1) to mild (grade 2) axonopathy was located in the dorsal white matter tracts, which project from DRG sensory neurons. This axonopathy was bilateral and characterized by dilated myelin sheaths with or without myelomacrophages, consistent with axonal degeneration (Figures 3D and 3E). We also observed axonal degeneration in the dorsal nerve roots of the spinal cord and in the sciatic nerve. The vehicle control did not have any axonopathy. Severity and incidence were dose dependent in the non-IS groups, whereas IS HD and IS LD animals were similarly affected (Figure 3F).

In the DRG, inflammatory cells were mostly $CD3^+$ T lymphocytes with fewer $CD20^+$ B lymphocytes (Figures 3B and 3C). Lymphocytes were clustered around hIDS-positive transduced neurons and sometimes formed small inflammatory nodules replacing missing neurons (neuronophagia). An increased density of nuclei not positive for lymphocyte or monocyte markers suggests that these were satellite cells that were activated to proliferate.

Two LD animals and one HD IS animal had minimal multifocal perivascular mononuclear cell infiltrates within brain parenchyma, meninges, choroid plexus, and/or neurohypophysis of the pituitary gland. The spinal cord gray matter was within normal limits in all animals.

### Vector Biodistribution

We quantified vector genomes in DNA extracted from the tissues listed in Table 2. See Table S7 for the complete biodistribution with individual results. Averages per group are shown in Figure 4A. We

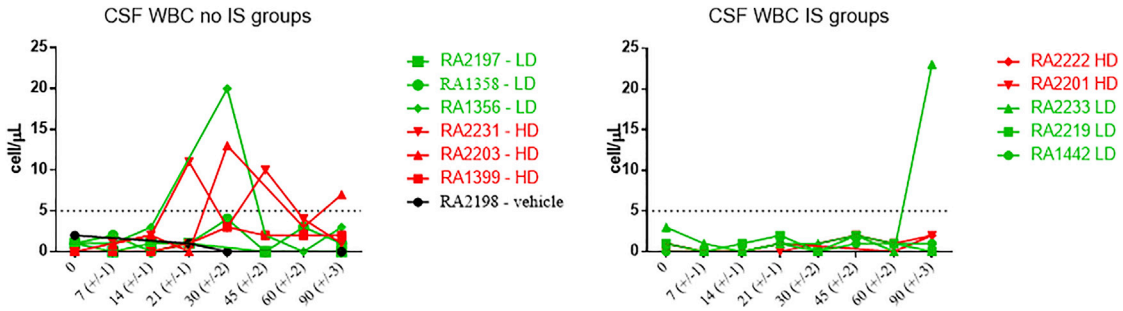


**Figure 1. CSF WBC Counts in Rhesus Macaques Injected with Suboccipital AAV9.hIDS**

Left panel, animals without IS; right panel, animals with IS (rapamycin and MMF with withdrawal of MMF on day 60). A minimal-to-mild CSF mononuclear pleocytosis (mainly lymphocytic) was observed in three HD, one LD, and one LD IS animal. The dashed line indicates the threshold for abnormal CSF cell counts in rhesus macaques (5 cells/µL CSF). Values were excluded when a blood contamination above 500 erythrocytes/µL was observed.

detected AAV vector genomes throughout the brain, spinal cord, and DRG of all vector-treated animals. GCs in the HD groups were between $1 \times 10^5$ and $1 \times 10^6$ GC/µg DNA in the brain, spinal cord segments, and DRG without a notable effect of the distance relative to the injection site in the spinal cord segments or DRG. Across all groups, we found that the lowest copy numbers from the CNS were in the cerebellum. Vector GC levels were similar or trended higher in the DRG from HD IS animals compared to HD animals.

The vector was significantly distributed to the peripheral organs, especially the liver, with GCs around 5 x $10^6$ GC/µg DNA in the HD group. We also recovered $1 \times 10^4$ to $1 \times 10^5$ GC/µg DNA vector genome from the heart and lymphoid organs (spleen, lymph nodes, and bone marrow). The lowest vector distribution was in the eye, kidney, gonads, lungs, and thyroid ($1 \times 10^2$ to $1 \times 10^3$ GC/µg). RA2233 had a baseline AAV9 NAb titer of 40 (Figure 2B) that completely inhibited transduction of the liver and heart (levels below the limit of detection in four lobes of the liver and 73.3 GC/µg DNA in the left lobe of the liver) but did not affect transduction of the brain, spinal cord, and DRG (Table S7).

### Vector DNA Shedding

We estimated vector shedding in the DNA extracted from urine and stools at baseline and days 5, 30, and 90. All animals shed vector DNA in their urine and stools 5 days after injection, most animals shed vector DNA in their stools 30 days after injection, and all animals had negative or close to the limit of detection values on day 90 (Figure 4B). Notably, given that we extracted DNA from samples using proteinase treatments and cell lysis, the recovery of vector DNA does not indicate the presence or absence of infective AAV particles.

### IDS Enzyme Activity in Serum and CSF

We periodically measured IDS activity in serum and CSF. CSF values were highly variable between time points and individuals, likely reflecting the instability of lysosomal enzymes in CSF (data not shown). Serum activity raised above baseline values in all but one animal on days 14 and 21. Values declined thereafter in the non-IS animals that developed anti-IDS antibodies. By contrast, values remained above baseline in the LD animal and all the IS animals that did not develop a significant anti-IDS humoral response (Figure S2). The enzyme activity of non-IS animals fell below baseline levels, suggesting that anti-hIDS antibodies interfered with the assay due to cross-reactivity with macaque IDS. Importantly, the LD IS animal that had preexisting AAV9 NAb and a complete inhibition of liver transduction did not present increased IDS activity at any time, suggesting that the peripheral serum enzyme activity is mainly a consequence of liver transduction.

## DISCUSSION

In this good-laboratory-practice-compliant study, we examined the safety of AAV9.hIDS gene transfer in nonhuman primates using a similar suboccipital route of administration as the one intended for first-in-human clinical trials. Notably, we observed no injection-procedure-related adverse events or histological lesions. In our experience, the usage of fluoroscopy image-guided confirmation of the needle placement allows a safe and reproducible method of administration in rhesus macaque, a nonhuman primate comparable in size to infants.

An important finding of this study was the presence of a subclinical sensory ganglionitis histologically similar to that observed in piglets or macaques administered systemically with an AAV9 variant encoding hSMN1[14] and in macaques receiving suboccipital administration of AAV9.hIDUA (see the related paper by Hordeaux et al.[15] in this issue of *Molceular Therapy - Methods & Clinical Development*).We do not know if the CSF pleocytosis that we observed in several species[14–16] is predictive of DRG toxicity, as it did not strictly correlate with histological findings in the animals. DRG neurons are highly transduced after both intrathecal and intravenous administration due to anatomic specificities. DRGs are outside of the blood-brain barrier and highly vascularized with fenestrated capillaries,[17,18] allowing direct access of AAV particles from the blood. DRGs are also bathed in CSF with direct access to AAV particles present in the intrathecal space through the pia mater or via axons of the dorsal nerve roots.

A

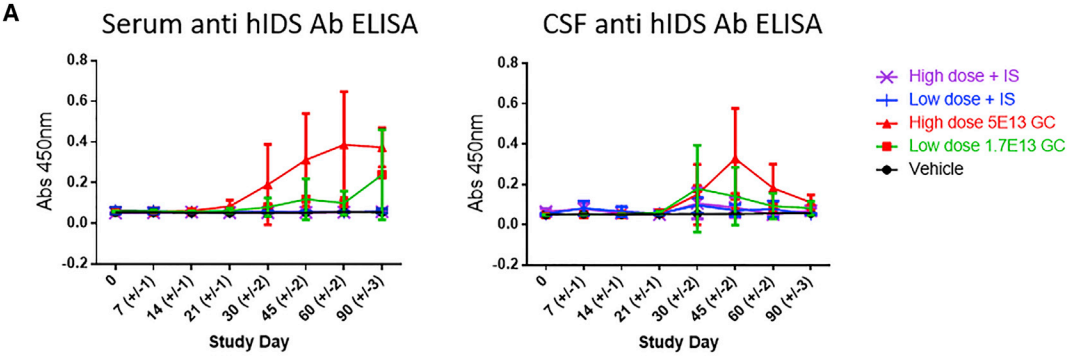


B

AAV9 neutralizing Ab titer

serum

| | Animal ID | BSL | D7 | D14 | D21 | D30 | D45 | D60 | D90 |
|---|---|---|---|---|---|---|---|---|---|
| Vehicle | RA2198 | <5 | <5 | <5 | 5 | <5 | <5 | <5 | <5 |
| LD | RA1356 | <5 | 40 | 80 | 160 | 160 | 320 | 320 | 320 |
| | RA1358 | <5 | 40 | 80 | 80 | 80 | 160 | 1280 | 640 |
| | RA2197 | <5 | 40 | 320 | 10 | 20 | 10 | 40 | 20 |
| HD | RA1399 | <5 | 160 | 1280 | 2560 | 640 | 2560 | 5120 | 2560 |
| | RA2203 | <5 | 160 | 320 | 160 | 320 | 2560 | 2560 | 2560 |
| | RA2231 | 5 | 5120 | 5120 | 5120 | 2560 | 2560 | 10240 | 5120 |
| LD IS | RA1442 | <5 | 20 | 10 | 10 | 10 | 10 | 160 | 80 |
| | RA2219 | <5 | 20 | 40 | 80 | 80 | 80 | 320 | 1280 |
| | RA2233 | 40 | 20 | 80 | 160 | 160 | 160 | 160 | 160 |
| HD IS | RA2201 | <5 | 10 | 10 | 20 | 20 | 20 | 20 | 160 |
| | RA2222 | <5 | <5 | 5 | <5 | <5 | <5 | 5 | 20 |

CSF

| | Animal ID | BSL | D7 | D14 | D21 | D30 | D45 | D60 | D90 |
|---|---|---|---|---|---|---|---|---|---|
| Vehicle | RA2198 | <5 | <5 | <5 | <5 | <5 | 20 | <5 | <5 |
| LD | RA1356 | <5 | <5 | <5 | <5 | <5 | 10 | 20 | 10 |
| | RA1358 | <5 | <5 | <5 | <5 | <5 | <5 | <5 | <5 |
| | RA2197 | <5 | <5 | <5 | <5 | <5 | <5 | 40 | <5 |
| HD | RA1399 | <5 | <5 | <5 | <5 | 10 | 10 | 10 | 10 |
| | RA2203 | <5 | <5 | <5 | <5 | <5 | 40 | 40 | 40 |
| | RA2231 | <5 | 5 | 5 | 40 | 80 | 40 | 20 | 20 |
| LD IS | RA1442 | <5 | <5 | <5 | <5 | <5 | <5 | <5 | <5 |
| | RA2219 | <5 | <5 | <5 | <5 | <5 | <5 | <5 | <5 |
| | RA2233 | <5 | <5 | <5 | <5 | <5 | <5 | <5 | <5 |
| HD IS | RA2201 | <5 | <5 | <5 | <5 | <5 | <5 | <5 | <5 |
| | RA2222 | <5 | <5 | <5 | <5 | <5 | <5 | <5 | <5 |

C

IFN-Y ELISPOT

| hIDS peptide pools | | PBMC | | | | | Spleen | Bone Marrow |
|---|---|---|---|---|---|---|---|---|
| | | BSL | D14 | D30 | D60 | D90 | D90 | D90 |
| Vehicle | RA2198 | - | - | - | - | - | - | - |
| LD | RA1356 | - | - | + | + | + | - | - |
| | RA1358 | - | - | - | - | - | - | - |
| | RA2197 | - | - | - | - | - | - | - |
| HD | RA1399 | - | - | - | - | - | - | - |
| | RA2203 | - | NC | - | - | - | - | - |
| | RA2231 | - | NC | - | - | - | - | - |
| LD IS | RA1442 | - | NC | - | - | - | - | - |
| | RA2219 | - | NC | - | - | - | - | - |
| | RA2233 | - | NC | - | - | - | - | - |
| HD IS | RA2201 | - | NC | - | - | - | - | - |
| | RA2222 | - | NC | - | - | - | - | - |

| AAV9 peptide pools | | PBMC | | | | | Spleen | Bone Marrow |
|---|---|---|---|---|---|---|---|---|
| | | BSL | D14 | D30 | D60 | D90 | D90 | D90 |
| Vehicle | RA2198 | - | - | - | - | - | - | - |
| LD | RA1356 | - | - | - | - | - | - | - |
| | RA1358 | - | - | - | - | - | - | - |
| | RA2197 | - | - | - | - | - | - | - |
| HD | RA1399 | - | - | - | - | - | - | - |
| | RA2203 | - | NC | - | - | - | - | - |
| | RA2231 | - | NC | - | - | - | - | - |
| LD IS | RA1442 | - | NC | - | - | - | + | - |
| | RA2219 | - | NC | - | + | + | + | - |
| | RA2233 | - | NC | + | - | - | - | - |
| HD IS | RA2201 | - | NC | - | - | - | - | - |
| | RA2222 | - | NC | - | - | - | - | - |

**Figure 2. Immune Responses to the Transgene Product and Capsid in Rhesus Macaques Injected with Suboccipital AAV9.hIDS**

(A) Serum (left) and CSF (right) anti-hIDS immune response measured by ELISA. Results are shown as averages per group with standard deviations as error bars. Humoral responses were low overall and were transient in the CSF. (B) AAV9 NAb titers in serum (left) and CSF (right). (C) Interferon-gamma ELISPOT responses in PBMCs, lymphocytes from spleen, and bone marrow toward hIDS transgene (left) and AAV9 capsid (right) peptide pools.

The mechanism of DRG neuron injury is unknown. The incidence and severity were lower in the present study, using AAV9.hIDS, compared to a similarly designed study using AAV9.hIDUA.[15] In the study evaluating AAV9.hIDUA, the highest dose of $1 \times 10^{13}$ GC was very close to the lowest dose of AAV9.hIDS ($1.7 \times 10^{13}$ GC), allowing direct comparison of both studies and suggesting a better safety profile of AAV9.hIDS at doses of approximately $1 \times 10^{11}$ GC per gram of brain. Immune responses to the transgene, both humoral and cellular, were also consistently lower with the hIDS transgene compared to hIDUA both in rhesus macaques and mice (unpublished data; Hinderer et al.[9]). This, as well as the presence of $CD20^+$ and $CD3^+$ lymphocytes in the affected DRGs, supports a role of the adaptive immune response in the physiopathology of the observed sensory ganglionitis. However, immune responses are probably not the only explanation, as IS did not prevent neuronal degeneration. Overexpression-related neuronal degeneration in nonhuman primates was recently reported by Golebiowski and colleagues[19] after intraparenchymal administration of AAV encoding hexosaminidase under the control of a ubiquitous strong promoter. Perhaps overexpression of a protein in DRG neurons induces a stress signal that triggers an initial low-grade neuronal injury and secretion of cytokines by the satellite cells and neurons.[20,21] Those cytokines, combined with the expression of a foreign protein, could trigger an adaptive immune response that would worsen the initial overexpression-related injury. This hypothesis shares similarities with paraneoplastic anti-Hu syndrome, in which a broken self-tolerance to the normally

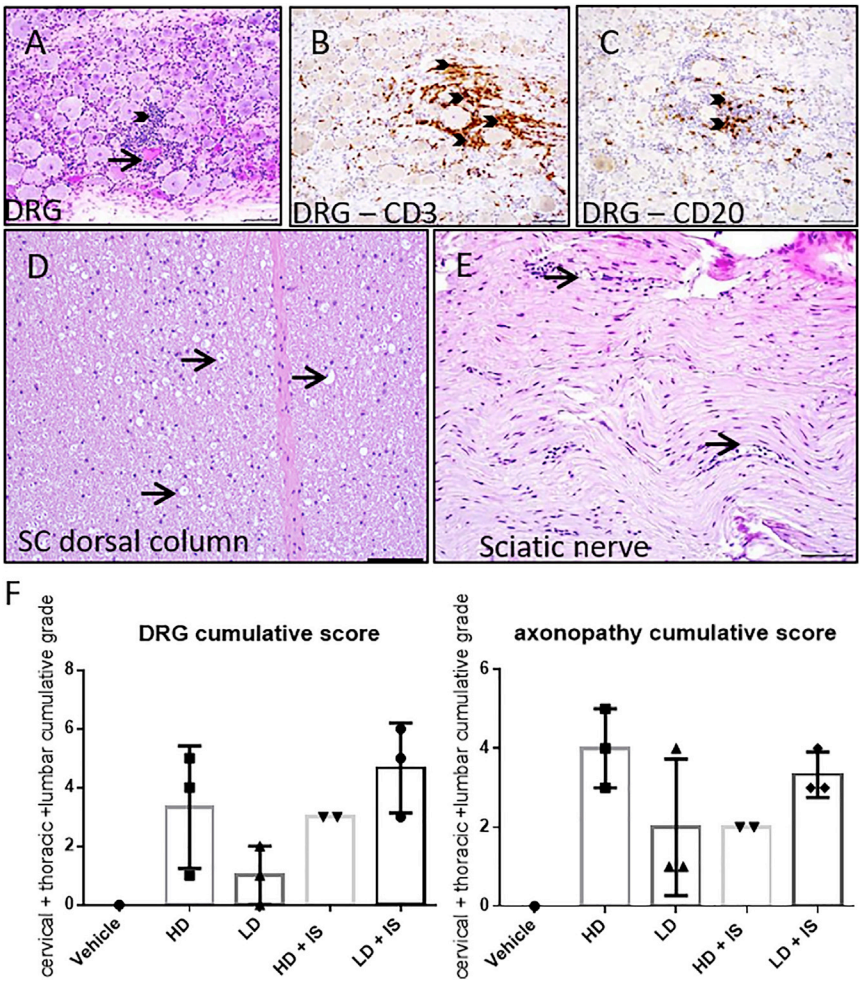


**Figure 3. Representative CNS and Peripheral Nervous System Histopathologic Findings in Rhesus Macaques Injected with Suboccipital AAV9.hIDS**

(A–C) The majority of animals had minimal-to-mild neuronal cell-body degeneration in the DRG characterized by neurodegeneration (arrow, A), satellitosis, and mononuclear cell infiltrates that surrounded and invaded neuronal cell bodies (arrowhead, A). Mononuclear cell infiltrates were predominantly composed of $CD3^+$ T cells (arrowheads, B) with fewer $CD20^+$ B cells (arrowheads, C). (D) All animals from test-article-treated groups had an axonopathy of the dorsal white matter tracts of the spinal cord, which was bilateral and characterized by dilated myelin sheaths with and without myelomacrophages (arrows), consistent with axonal degeneration. (E) In a few animals, a similar axonopathy (arrows) was observed in the sciatic nerve. H&E, scale bars, 200 μm (A), 100 μm (D and E). CD3 or CD20 IHC, scale bars, 100 μm (B and C). (F) Individual DRG (left) and axonopathy (right) cumulative scores defined as the sum of cervical, thoracic, and lumbar segment scores with 1 as minimal, 2 as mild, 3 as moderate, 4 as marked, and 5 as severe; no animal had a score higher than 2 in any analyzed segment. Error bars represent standard deviation.

neuron-restricted Hu antigen causes an immune-mediated sensory ganglionitis that is strikingly similar on histological examination.[22,23]

Another interesting finding of this study is the effect of preexisting low titers of serum AAV9 NAb on the biodistribution and the effect of anti-IDS or anti-drug antibodies (ADAs) on enzyme activity. Substantial quantities of vector distribute outside of the CNS and deposit in organs such as the liver and spleen after intrathecal vector administration across species.[7–9,24–26] One animal presented at baseline with serum NAb titer equal to 40, whereas the rest were NAb negative, providing an opportunity to evaluate the impact of preexisting NAbs on vector distribution within and outside of the CNS. Transduction of liver was completely inhibited in the animal with preexisting serum Nabs, whereas there was no change in CNS transduction. This is likely due to asymmetric distribution of NAbs between the systemic and CNS compartments observed by us and others.[24,25] The fact that DRG transduction was also not impacted suggests that AAV particles gained entry via the CSF rather than the fenestrated endothelium of the DRG. Further studies are needed to define a safe range of baseline NAb that will allow efficient CNS transduction with minimal peripheral off-target transduction, without risking adverse events triggered by immune complexes. In the context of lysosomal storage disorders, the liver secretion of enzymes is beneficial for the systemic manifestations of the disease. Patients with baseline NAbs that may be treated with intrathecal gene therapy will likely continue to rely on a peripheral source of enzymes, such as systemic ERT, to manage some aspects of their disease. The formation of ADAs to hIDS led to the decrease and loss of measurable hIDS activity in the serum of non-IS animals, whereas IS animals maintained a sustained increased activity. The impact of circulating antibodies on the efficacy of gene therapy is unknown. In a feline model of mucopolysaccharidosis type I (MPS I), the ADAs elicited after intrathecal AAV9.fIDUA gene therapy caused a decrease of enzyme activity in the fluids of some animals, whereas biomarkers of therapy efficacy demonstrated a persistent biochemical response to gene transfer.[8] On the contrary, when using hIDUA in a canine model of MPS I, inducing immune tolerance to the transgene was necessary for therapeutic efficacy, perhaps due to an exaggerated immune response toward a foreign transgene.[16] Therefore, we caution the use of enzyme activity in the serum as a biomarker of gene transfer efficacy; only early time points may be informative in patients who will develop ADAs, and it may not be feasible in patients with past exposure to ERT.

Overall, this study of intrathecal AAV9.hIDS in rhesus macaque demonstrated safety of the suboccipital vector administration procedure as well as an overall positive benefit-risk profile in the severe

A

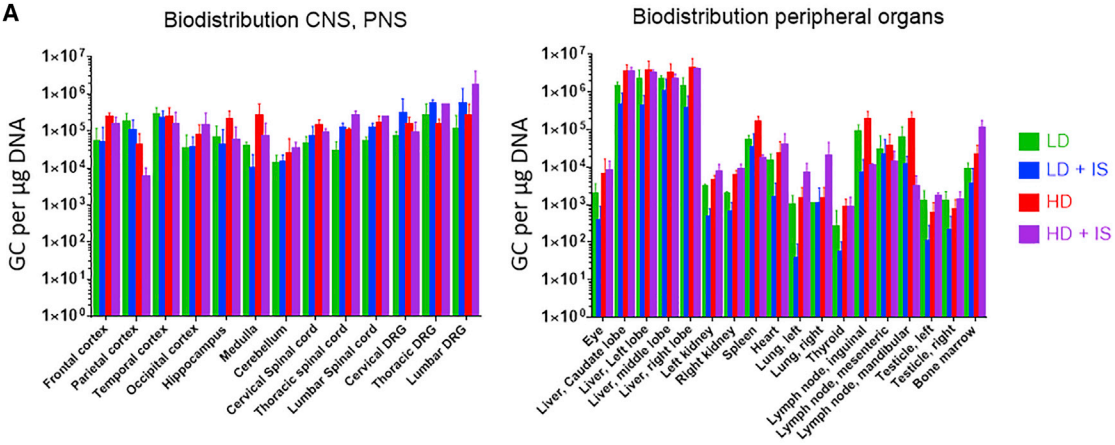


B

| | | Shedding in urine GC/12µL | | | | Shedding in stools GC/µDNA | | | |
|---|---|---|---|---|---|---|---|---|---|
| | Animal ID | BSL | D5 | D30 | D90 | BSL | D5 | D30 | D90 |
| Vehicle | RA2198 | < 25 | < 25 | < 25 | < 25 | < 50 | < 50 | < 50 | < 50 |
| LD | RA1356 | < 25 | 191.15 | < 25 | < 25 | < 50 | 185,021 | < 50 | < 50 |
| | RA1358 | 48.88 | 84.32 | < 25 | < 25 | < 50 | 32,322 | < 50 | < 50 |
| | RA2197 | < 25 | 155.22 | < 25 | < 25 | < 50 | 106,035 | 96.01 | < 50 |
| HD | RA1399 | < 25 | 1199.01 | < 25 | < 25 | < 50 | 201,658 | 114.96 | 79.8 |
| | RA2203 | < 25 | 94.86 | < 25 | < 25 | < 50 | 43,480 | 61.34 | < 50 |
| | RA2231 | < 25 | 827.15 | < 25 | < 25 | < 50 | 206,496 | 108.97 | < 50 |
| LD IS | RA1442 | < 25 | 1,003.50 | < 25 | < 25 | < 50 | 87,834 | < 50 | < 50 |
| | RA2219 | < 25 | 1,449.10 | < 25 | < 25 | < 50 | 188,642 | < 50 | < 50 |
| | RA2233 | < 25 | 164.5 | < 25 | < 25 | < 50 | 26,922 | < 50 | < 50 |
| HD IS | RA2201 | < 25 | 1,584.00 | < 25 | < 25 | < 50 | 5,975,492 | 125 | < 50 |
| | RA2222 | 99.9 | 40,526.60 | 34.9 | < 25 | < 50 | 5,136,848 | 100 | < 50 |

**Figure 4. Biodistribution in Tissues, Urine, and Stools in Rhesus Macaques Injected with Suboccipital AAV9.hIDS**

(A) Vector GCs in the central and peripheral nervous systems (left) and peripheral organs (right) 90 days after vector administration. Averages per group with SD as error bars. (B) Vector GC shedding in urine (GC/12 µL urine, limit of detection 25 GC) and stools (GC/µg DNA, limit of detection 50 GC) at baseline and days 5, 30, and 90.

Hunter population. The toxicity observed in this study was limited to minimal-to-moderate DRG neuron lesions, comparable to what was observed with ICM AAV9.hIDUA but with decreased incidence and severity at similar doses. The better nonclinical safety profile of AAV9.hIDS compared to AAV9.hIDUA may be due to the overall reduced immunogenicity of hIDS compared to hIDUA that we noted in early mouse studies (unpublished data; Hinderer et al.[9]). The treatment-related minimal-to-mild sensory ganglionitis in nonhuman primates warrants informed consent as well as careful monitoring of patients during first-in-human trials using electrophysiological recordings of sensory neurons and nerves.

## MATERIALS AND METHODS

### Animals

All animal procedures were approved by the Institutional Animal Care and Use Committee of the University of Pennsylvania, and all experiments conform to all relevant regulatory standards. Rhesus macaques (*Macaca mulatta*) that screened negative for AAV9 NAbs were purchased from Covance Research Products (Denver, PA). They were housed in an Association for Assessment and Accreditation of Laboratory Animal Care International-accredited Nonhuman Primate Research Program facility at the University of Pennsylvania in stainless-steel squeeze-back cages and were given varied enrichments (e.g., food treats, visual and auditory stimuli, manipulatives, social interactions).

### Study Design

This paper combines two studies; overviews of the study design and animals are presented in Table 1 and Table 2, respectively. We designed these studies to evaluate the safety, biodistribution, and pharmacology of two dose levels of test article, a vector encoding hIDS, for up to 90 days after administration by image-guided suboccipital puncture in rhesus macaques. The first study included seven animals and the second six animals that were immunosuppressed using a combination of rapamycin and MMF. All animals were males because of the X-linked nature of Hunter syndrome and were randomly assigned to their group using an online randomized number generator (https://www.random.org/). The IS regimen caused adverse effects of

**Table 3. Tissues Sampled at Necropsy**

| | | |
|---|---|---|
| Tissues Collected for Histopathology | | |
| Adrenal gland, left | liver, all lobes | small intestine, duodenum |
| Adrenal gland, right | lung, left | small intestine, jejunum |
| Ascending aorta (proximal) | lung, right | small intestine, ileum (Peyers patch) |
| Bone marrow, rib | lacrimal gland | spinalcord |
| Brain | lymph node, mandibular | spleen |
| Cecum | lymph node, mesenteric | stomach |
| Dorsal root ganglia | lymph node, inguinal | testes |
| Epididymides | muscle, quadriceps femoris | urinary bladder |
| Esophagus | pancreas | pituitary |
| Eye, left | prostate | thymus |
| Gall bladder | rectum | thyroid gland (with parathyroid) |
| Heart | salivary gland, mandibular | trachea |
| Injection site (muscle, skin) | sciatic nerves | trigeminal nerve ganglia, right |
| Kidney, left | seminal vesicle | gross lesions (if any) |
| Kidney, right | skin with mammary | – |
| Large intestine, colon | – | – |
| Tissues Collected for Biodistribution | | |
| Bone marrow, femur | kidney, right | spinal cord, thoracic |
| Brain, cerebellum | liver, caudate lobe | spinal cord, lumbar |
| Brain, frontal cortex | liver, left lobe | spleen |
| Brain, hippocampus | liver, middle lobe | testicle, left |
| Brain, medulla | liver, right lobe | testicle, right |
| Brain, occipital cortex | lung, left | dorsal root ganglia |
| Brain, parietal cortex | lung, right | trigeminal nerve ganglion, left |
| Brain, temporal cortex | lymph node, mandibular | thyroid gland (with parathyroid) |
| Eye, right | lymph node, mesenteric | gross lesion (if any) |
| Heart | lymph node, inguinal | – |
| Kidney, left | spinal cord, cervical | – |
| Tissues Collected for Lymphocyte Isolation | | |
| Spleen | bone marrow | – |

diarrhea, which led to the removal of one animal prior to test article dosing in the HD IS group. Control article (artificial CSF) was administered via suboccipital puncture to a single macaque in group 1. Test article formulated in artificial CSF was administered via suboccipital puncture to 11 rhesus macaques. These animals were randomized to receive either a HD of $5 \times 10^{13}$ GCs (n = 5) or an LD of $1.7 \times 10^{13}$ GCs (n = 6) with or without IS. Blood and CSF were collected as part of a general safety panel at baseline and days 7, 14, 21, 30, 45, 60, and 90. hIDS enzymatic activity and the humoral response to the hIDS transgene product and to the AAV9 capsid were analyzed in serum and CSF at the same time points. T cell responses to the hIDS transgene product and to the AAV9 capsid were evaluated at baseline and days 14, 30, 60, and 90 in the blood, and at day 90 in spleen and bone marrow. Vector genomes were quantified in urine and feces (shedding) at baseline and days 5, 30, and 90. Following completion of the in-life phase of the study at 90 ± 3 days post-vector administration, macaques were euthanized with intravenous pentobarbital overdose and necropsied. Tissues were harvested for comprehensive histopathologic evaluation and biodistribution analysis (Table 3).

### Test Article

The test article consisted of an AAV9 capsid packaging an expression construct with a hybrid promoter (the cytomegalovirus enhancer with a chicken beta actin promoter), a chicken beta actin intron, the hIDS transgene, and a rabbit beta-globulin polyadenylation signal. The expression construct was flanked by AAV2 inverted terminal repeats and was cloned in a plasmid containing a kanamycin resistance gene for manufacturing. The test article was manufactured under conditions as similar as possible to good manufacturing practice guidelines. The

vector was produced by triple transfection of adherent HEK293 cells and purified from supernatant by affinity chromatography using a POROS CaptureSelect AAV9 resin (Thermo Fisher Scientific, Waltham, MA), followed by anion exchange chromatography. Sterility of the test article was verified by a direct immersion assay. Limulus amebocyte lysate and qPCR tests for endotoxin and mycoplasma, respectively, were negative. Vector titer by TaqMan PCR was $5.72 \times 10^{13}$ GC/mL (average result of n = 3). The purity of capsid proteins was 97.86% of viral proteins, as determined by SDS-PAGE analysis. Analytical ultracentrifugation indicated that the preparation contained a 2.1:1 full:empty particle ratio. *In vitro* potency of the vector, assessed by IDS enzyme expression, was confirmed to be similar to reference vector lots. The final product was diluted in Elliott's B Solution (Lukare Medical, Scotch Plain, NJ) with 0.001% Pluronic F-68 (Thermo Fisher Scientific, Waltham, MA). Dilutions were calculated using a standardized vector preparation form, and calculations were verified by designated personnel as indicated on the vector preparation forms. Unused vector preparations were archived and stored at −60°C to 80°C.

### ICM Injection Procedure

Anesthetized macaques were transferred from animal holding to the procedure room and placed on an X-ray table in the lateral decubitus position with the head flexed forward for CSF collection and dosing ICM. The site of injection was aseptically prepared. Using aseptic technique, a 21G–27G, 1–1.5-inch Quincke spinal needle (Becton Dickinson, Franklin Lakes, NJ) was advanced into the suboccipital space until the flow of CSF was observed, and 1 mL of CSF was collected for baseline analysis. The needle was directed at the wider superior portion of the cisterna magna to avoid potential brainstem injury; correct needle placement was verified by fluoroscopy (OEC 9800 C-arm; GE Healthcare, Little Chalfont, UK). After CSF collection, a Luer access extension catheter was connected to the spinal needle to facilitate dosing of 1 mL of 180 mg/mL Iohexol contrast media (GE Healthcare, Little Chalfont, UK). After verifying needle placement, a syringe containing the test article (volume equivalent to 1 mL plus the syringe volume and linker dead space) was connected to the flexible linker and injected over 30 ± 5 s. The needle was removed, and direct pressure was applied to the puncture site.

Verification of correct placement of the needle using a computed tomography scanner and contrast injection is key to mitigate the risk of accidental puncture or injection into the brainstem. This procedure, when translated to patients, will be performed in neurointerventional radiology suites and will use both angiography and intrathecal contrast injection to prevent accidental puncture of large vessels or brainstem.

### Immunosuppression

A pilot study was conducted and demonstrated that orogastric gavage in chair-trained animals was a more reliable and reproducible method to achieve and maintain blood and plasma trough target levels when compared to treat-based voluntarily consumption. Animals were acclimated to the collar, pole capture, and chair restraint. Once acclimated, the animals were trained for insertion of an orogastric feeding tube and were then dosed through the feeding tube with a combination of commercially available IS drugs: a 200 mg/mL oral solution of MMF (Cellcept, Roche Products) and 0.5, 1, or 2 mg coated tablets of rapamycin (aka Sirolimus, Rapamune, Greenstone) crushed in water. The IS regimen was started 3 weeks prior to intrathecal dosing of the test article. Rapamycin (0.75–2 mg/kg, once per day) and MMF (25–100 mg/kg, twice per day) doses were adjusted to maintain a blood target trough level range of 2–3.5 μg/mL of mycophenolic acid and 10–15 μg/L of rapamycin. Rapamycin was used for the entirety of the study, whereas MMF was stopped on study day 60. Trough levels were monitored twice a week, and IS doses were adjusted if the levels were either below or above the target range for two consecutive bleedings. Overall, rapamycin levels were steady and on target.

### Blood and CSF Analysis

Serum chemistry, hematology, coagulation, and CSF analyses were performed by the contract facility Antech GLP or Antech Diagnostics (Morrisville, NC).

### Immunology

Peripheral blood T cell responses against hIDS and the AAV9 capsid were measured by interferon gamma enzyme-linked immunosorbent spot (ELISPOT) assays according to previously published methods[11] using peptide libraries specific for the AAV9 capsid and the hIDS transgene. Positive response criteria were >55 spot-forming units per $10^6$ lymphocytes and three times the medium negative control upon no stimulation. In addition, the T cell response was assayed in lymphocytes that were extracted from spleen and bone marrow after necropsy on study day 90. NAbs against AAV9 capsid were measured in serum and CSF as previously described[27] using an *in vitro* HEK293 cell-based assay. NAb titers are reported as the reciprocal of the sample dilution that inhibits transduction of 50% of the cells. The limit of detection of the assay was 1:5 sample dilution. Antibodies to hIDS were measured in serum and CSF as previously described.[9]

### Enzyme Activity

IDS activity was detected by conversion of the substrate 4-methylumbelliferyl α-L-idopyranosiduronic acid 2-sulfate to the fluorescent product 4-methylumbelliferone in a two-step process. In brief, serum was diluted 1:20 and CSF 1:5 in PBS. 10 μL of diluted sample was incubated with 20 μL of substrate solution at pH 5.0. In this step, IDS cleaves the sulfate moiety from the substrate. Duplicate samples were incubated for 1 and 3 hr at 37°C; laronidase (Aldurazyme) was then added and incubated at 37°C overnight to complete the conversion of the desulfated substrate into the fluorescent 4-methylumbelliferone product. Next, 20 μL of the reaction mix was transferred to a black 96-well plate, and 180 μL of stop solution (pH 10.9) was added. Fluorescence was measured at 365 nm for excitation and 450 nm for emission. The final concentration of the reaction product for each sample was determined from a 4-methylumbelliferone (4-MU) standard curve and expressed as concentration of 4-MU per unit of time and volume. Baseline sample values, representing endogenous macaque IDS activity, were subtracted to obtain activity resulting from the transgene hIDS.

### Biodistribution and Shedding

DNA from urine was isolated using QIAamp Viral RNA Mini Extraction kits (QIAGEN, Germantown, MD); DNA from fecal samples and tissues were isolated using QIAamp DNA Stool Mini kits (QIAGEN, Germantown, MD) and QIAamp columns (QIAGEN, Germantown, MD), respectively. Biodistribution analysis was performed by TaqMan qPCR targeting a vector polyadenylation signal sequence. Assay results were reported as GC/12 μL urine or GC/μg of DNA (stools).

### Histology

Tissues were fixed in formalin, paraffin embedded, sectioned, and stained with H&E according to standard protocols. Tissues were evaluated histologically and peer-reviewed by two board-certified veterinary anatomic pathologists. The severity of lesions were graded as follows: grade 1 (minimal histopathologic change from inconspicuous to barely noticeable, affecting less than approximately 10% of the tissue); grade 2 (mild histopathologic change that is noticeable but not prominent, affecting approximately 10% to 25% of the tissue); grade 3 (moderate histopathologic change that is prominent but not a dominant feature, affecting approximately 25% to 50% of the tissue); grade 4 (marked histopathologic change that is dominant but not an overwhelming feature, affecting approximately 50% to 95% of the tissue); grade 5 (severe histopathologic change that is an overwhelming feature, affecting greater than approximately 95% of the tissue). Three segments of the spinal cord (cervical, thoracic, lumbar), and at least three DRGs from each segment (cervical, thoracic, lumbar) were evaluated. To ease global interpretation and allow comparison between groups, we also present combined scores for the spinal cord and DRG findings, representing the sum of the severity grades in cervical, thoracic, and lumbar segments with a range of 0 to 15.

For immunohistochemistry to detect T (CD3) and B (CD20) lymphocytes, paraffin sections were deparaffinized through a series of xylene and ethanol treatments, boiled in a microwave for 6 min in 10 mM citrate buffer (pH 6.0), and treated sequentially with 2% $H_2O_2$ (15 min; Sigma-Aldrich, St. Louis, MO), avidin-biotin blocking reagents (15 min each; Vector Laboratories, Burlingame, CA), and blocking buffer (1% donkey serum in PBS + 0.2% Triton for 10 min) followed by incubation with primary (1 hr) and biotinylated secondary antibodies (45 min; donkey antibodies from Jackson ImmunoResearch, West Grove, PA) diluted in blocking buffer. Primary antibodies were rabbit polyclonal against CD3 (A045229-2; Agilent Technologies, Santa Clara, CA) and CD20 (PA5-16701; Life Technologies, Carlsbad, CA). A Vectastain Elite ABC kit (Vector Laboratories, Burlingame, CA) was used with 3,3′-diaminobenzidine as the substrate to visualize bound antibodies as brown precipitate, and sections were slightly counterstained with hematoxylin to show nuclei.

## SUPPLEMENTAL INFORMATION

Supplemental Information includes two figures and seven tables and can be found with this article online at https://doi.org/10.1016/j.omtm.2018.06.004.

## AUTHOR CONTRIBUTIONS

J.H. performed study design, investigation, data analysis, and writing; C.H. performed study design and writing; T.G. conducted animal dosing and veterinary care; E.L.B. and L.K.R. performed histopathology; P.B. supervised histology, immunohistochemistry, and immunofluorescence; R.C. supervised immune response analysis; L.K.R. supervised the studies; and J.M.W. was responsible for conceptualization and supervision of the studies.

## CONFLICTS OF INTEREST

J.M.W. is an advisor to, holds equity in, and has a sponsored research agreement with REGENXBIO; he also has a sponsored research agreement with Ultragenyx, Biogen, and Janssen, which are licensees of Penn technology. J.M.W. holds equity in Solid Bio and is an inventor on patents that have been licensed to various biopharmaceutical companies.

## ACKNOWLEDGMENTS

This work was funded by REGENXBIO. We would like to thank Shu-Jen Chen and Michael Korn for the shedding and biodistribution studies and Jessica Chichester for immune response interpretation. Invaluable technical assistance was provided by the Nonhuman Primate Research Program, the Immunology Core, Vector Clinical Services, the Vector Core, and the Morphology Core of the Gene Therapy Program of the University of Pennsylvania.

## REFERENCES

1. Tomanin, R., Zanetti, A., D'Avanzo, F., Rampazzo, A., Gasparotto, N., Parini, R., Pascarella, A., Concolino, D., Procopio, E., Fiumara, A., et al. (2014). Clinical efficacy of enzyme replacement therapy in paediatric Hunter patients, an independent study of 3.5 years. Orphanet J. Rare Dis. *9*, 129.

2. Neufeld, E.F., and Muenzer, J. (2001). The mucopolysaccharidoses. In The Metabolic & Molecular Bases of Inherited Disease, C. Scriver, A. Beaudet, and W. Sly, eds. (McGraw-Hill), pp. 3421–3452.

3. Crowe, L., Yaplito-Lee, J., Anderson, V., and Peters, H. (2017). Cognitive and behaviour profiles of children with mucopolysaccharidosis Type II. Cogn. Neuropsychol. *34*, 347–356.

4. Parini, R., Rigoldi, M., Tedesco, L., Boffi, L., Brambilla, A., Bertoletti, S., Boncimino, A., Del Longo, A., De Lorenzo, P., Gaini, R., et al. (2015). Enzymatic replacement therapy for Hunter disease: Up to 9 years experience with 17 patients. Mol. Genet. Metab. Rep. *3*, 65–74.

5. Muenzer, J., Hendriksz, C.J., Fan, Z., Vijayaraghavan, S., Perry, V., Santra, S., Solanki, G.A., Mascelli, M.A., Pan, L., Wang, N., et al. (2016). A phase I/II study of intrathecal idursulfase-IT in children with severe mucopolysaccharidosis II. Genet. Med. *18*, 73–81.

6. Hendriksz, C.J., Muenzer, J., Vanderver, A., Davis, J.M., Burton, B.K., Mendelsohn, N.J., Wang, N., Pan, L., Pano, A., and Barbier, A.J. (2015). Levels of glycosaminoglycans in the cerebrospinal fluid of healthy young adults, surrogate-normal children, and Hunter syndrome patients with and without cognitive impairment. Mol. Genet. Metab. Rep. *5*, 103–106.

7. Hinderer, C., Bell, P., Katz, N., Vite, C., Louboutin, J.-P., Bote, E., Hongwei, Y., Yanqing, Z., Casal Margaret, L., Bagel, J., et al. (2018). Evaluation of intrathecal routes of administration for adeno-associated virus vectors in large animals. Hum. Gene Ther. *29*, 15–24.

8. Hinderer, C., Bell, P., Gurda, B.L., Wang, Q., Louboutin, J.P., Zhu, Y., Bagel, J., O'Donnell, P., Sikora, T., Ruane, T., et al. (2014). Intrathecal gene therapy corrects CNS pathology in a feline model of mucopolysaccharidosis I. Mol. Ther. *22*, 2018–2027.

9. Hinderer, C., Katz, N., Louboutin, J.-P., Bell, P., Yu, H., Nayal, M., Kozarsky, K., O'Brien, W.T., Goode, T., and Wilson, J.M. (2016). Delivery of an Adeno-Associated Virus Vector into Cerebrospinal Fluid Attenuates Central Nervous System Disease in Mucopolysaccharidosis Type II Mice. Hum. Gene Ther. *27*, 906–915.

10. Gurda, B., Wang, P., Bell, P., Bagel, J., Sikora, T., O'Donnell, P., Zhu, Y., Yu, H., Ruane, T., Calcedo, R., et al. (2014). Evaluation of intrathecal rAAV vectors in canine Mucopolysaccharidosis VII. Mol. Ther. *22*, S100–S101.

11. Gao, G., Wang, Q., Calcedo, R., Mays, L., Bell, P., Wang, L., Vandenberghe, L.H., Grant, R., Sanmiguel, J., Furth, E.E., and Wilson, J.M. (2009). Adeno-associated virus-mediated gene transfer to nonhuman primate liver can elicit destructive transgene-specific T cell responses. Hum. Gene Ther. *20*, 930–942.

12. Wang, L., Calcedo, R., Wang, H., Bell, P., Grant, R., Vandenberghe, L.H., Sanmiguel, J., Morizono, H., Batshaw, M.L., and Wilson, J.M. (2010). The pleiotropic effects of natural AAV infections on liver-directed gene transfer in macaques. Mol. Ther. *18*, 126–134.

13. Greig, J.A., Limberis, M.P., Bell, P., Chen, S.-J., Calcedo, R., Rader, D.J., and Wilson, J.M. (2017). Non-Clinical Study Examining AAV8.TBG.hLDLR Vector-Associated Toxicity in Chow-Fed Wild-Type and LDLR$^{+}$/− Rhesus Macaques. Hum. Gene Ther. Clin. Dev. *28*, 39–50.

14. Hinderer, C., Katz, N., Buza, E.L., Dyer, C., Goode, T., Bell, P., Richman, L.K., and Wilson, J.M. (2018). Severe Toxicity in Nonhuman Primates and Piglets Following High-Dose Intravenous Administration of an Adeno-Associated Virus Vector Expressing Human SMN. Hum. Gene Ther. *29*, 285–298.

15. Hordeaux, J., Hinderer, C., Goode, T., Katz, N., Buza, E.L., Bell, P., et al. (2018). Toxicology Study of Intrathecal Adeno-Associated Virus 9 expressing Human Alpha-L-Iduronidase in Rhesus Macaques. Mol. Ther. Methods Clin. Dev. *10*. Published online September 9, 2018. https://doi.org/10.1016/j.omtm.2018.06.003.

16. Hinderer, C., Bell, P., Louboutin, J.P., Zhu, Y., Yu, H., Lin, G., Choa, R., Gurda, B.L., Bagel, J., O'Donnell, P., et al. (2015). Neonatal Systemic AAV Induces Tolerance to CNS Gene Therapy in MPS I Dogs and Nonhuman Primates. Mol. Ther. *23*, 1298–1307.

17. Jimenez-Andrade, J.M., Herrera, M.B., Ghilardi, J.R., Vardanyan, M., Melemedjian, O.K., and Mantyh, P.W. (2008). Vascularization of the dorsal root ganglia and peripheral nerve of the mouse: implications for chemical-induced peripheral sensory neuropathies. Mol. Pain *4*, 10.

18. Godel, T., Pham, M., Heiland, S., Bendszus, M., and Bäumer, P. (2016). Human dorsal-root-ganglion perfusion measured in-vivo by MRI. Neuroimage *141*, 81–87.

19. Golebiowski, D., van der Bom, I.M.J., Kwon, C.S., Miller, A.D., Petrosky, K., Bradbury, A.M., Maitland, S., Kühn, A.L., Bishop, N., Curran, E., et al. (2017). Direct Intracranial Injection of AAVrh8 Encoding Monkey β-N-Acetylhexosaminidase Causes Neurotoxicity in the Primate Brain. Hum. Gene Ther. *28*, 510–522.

20. Austin, P.J., and Moalem-Taylor, G. (2010). The neuro-immune balance in neuropathic pain: involvement of inflammatory immune cells, immune-like glial cells and cytokines. J. Neuroimmunol. *229*, 26–50.

21. Moalem, G., and Tracey, D.J. (2006). Immune and inflammatory mechanisms in neuropathic pain. Brain Res. Brain Res. Rev. *51*, 240–264.

22. Pignolet, B.S.L., Gebauer, C.M.T., and Liblau, R.S. (2013). Immunopathogenesis of paraneoplastic neurological syndromes associated with anti-Hu antibodies: A beneficial antitumor immune response going awry. OncoImmunology *2*, e27384.

23. Bernal, F., Graus, F., Pifarré, A., Saiz, A., Benyahia, B., and Ribalta, T. (2002). Immunohistochemical analysis of anti-Hu-associated paraneoplastic encephalomyelitis. Acta Neuropathol. *103*, 509–515.

24. Gray, S.J., Nagabhushan Kalburgi, S., McCown, T.J., and Jude Samulski, R. (2013). Global CNS gene delivery and evasion of anti-AAV-neutralizing antibodies by intrathecal AAV administration in non-human primates. Gene Ther. *20*, 450–459.

25. Haurigot, V., Marcó, S., Ribera, A., Garcia, M., Ruzo, A., Villacampa, P., Ayuso, E., Añor, S., Andaluz, A., Pineda, M., et al. (2013). Whole body correction of mucopolysaccharidosis IIIA by intracerebrospinal fluid gene therapy. J. Clin. Invest. *123*, 3254–3271.

26. Hinderer, C., Bell, P., Louboutin, J.P., Katz, N., Zhu, Y., Lin, G., Choa, R., Bagel, J., O'Donnell, P., Fitzgerald, C.A., et al. (2016). Neonatal tolerance induction enables accurate evaluation of gene therapy for MPS I in a canine model. Mol. Genet. Metab. *119*, 124–130.

27. Calcedo, R., Vandenberghe, L.H., Gao, G., Lin, J., and Wilson, J.M. (2009). Worldwide epidemiology of neutralizing antibodies to adeno-associated viruses. J. Infect. Dis. *199*, 381–390.